Available online at www.sciencedirect.com
SCIENCE DIRECT
Journal of Nuclear Materials 351 (2006) 109–118
journal of nuclear materials
www.elsevier.com/locate/jnucmat

Calculation of helium defect clustering properties in iron using a multi-scale approach

T. Seletskaia [a], Yu.N. Osetsky [b], R.E. Stoller [a,*], G.M. Stocks [a]

[a] *Metals and Ceramics Division, Oak Ridge National Laboratory, Building 4500S, MS-6138, P.O. Box 2008, Oak Ridge, TN 37831-6138, United States*
[b] *Computer Science and Mathematics Division, Oak Ridge National Laboratory, Oak Ridge, TN 37831-6138, United States*

Abstract

Electronic structure calculations were used to study the relaxation, formation and binding energies of small helium clusters in iron. We considered three He defect configurations: two He atoms in an interstitial position and two and three He atoms located in one vacancy. To study He–vacancy clusters containing more He atoms, we used a multi-scale approach and constructed an empirical potential fitted to both formation and relaxation energies of a single He defect and small He clusters obtained from the first principles calculations. The potential consists of a repulsive pair-interaction part and a many-body attractive term describing the cohesion. The potential was used to study stability of He–vacancy clusters at zero temperature. The binding energy of a He atom to a He-cluster varies from 1.3 eV to 1.9 eV depending on the cluster size. When more than six He atoms are placed into a vacancy an Fe self-interstitial atom (SIA) is produced. The SIA binding energy to a He–di-vacancy cluster decreases from 5.0 eV to 0.7 eV as the number of He atoms increases. The results obtained are consistent with experimental observations of helium desorption reported in the literature.

1. Introduction

Helium is produced in neutron-irradiated metals as the result of (n,α) transmutation reactions [1]. Experiments show [2,3] that it is deeply trapped by the vacancies, decreasing vacancy mobility and enhancing accumulation of additional vacancies and helium atoms [4]. This process leads to helium bubble formation, which can promote void swelling with a volume change potentially reaching several tens of percent [5].

Understanding the fundamental behavior of helium in metals is one of the key issues in the research and development of fusion reactor materials. However, due to helium's high interstitial mobility and tendency to bind strongly with vacancies, information on its atomistic behavior is hard to assess from experiments. The main problem is absence of information on properties and mechanisms such as He migration via the interstitial or vacancy mechanism, binding properties of He–vacancy clusters, etc., which are necessary for interpretation of experimental data. The only way to obtain such information is atomic-scale modeling via ab initio and/or classical molecular dynamics/statics techniques. A few attempts have been made

* Corresponding author. Tel.: +1 865 576 788; fax: +1 865 241 3650.
E-mail address: rkn@ornl.gov (R.E. Stoller).

0022-3115/$ - see front matter © 2006 Elsevier B.V. All rights reserved.
doi:10.1016/j.jnucmat.2006.02.016

so far and the majority of calculations performed [6–10] were based on empirical pair potentials for He in metals, particularly in Fe, as constructed by Wilson [11] in the late 1960s. The Fe potential was calculated using the modified Wedepohl [12] method based on the Thomas–Fermi–Dirac formalism. The exchange energy of the electrons was treated within the homogeneous gas approximation, ignoring correlation effects. The potential was defined based on a pairwise interaction energy for an Fe–He^0 dimer completely ignoring bulk properties of the matrix. The latter makes it inappropriate for simulating energy and dynamic properties of He defects in the iron matrix.

Electronic structure ab initio calculations [13,14] based on the density functional theory (DFT) [15,16] have demonstrated that the Wilson potential [6–8] and other empirical models [9,10] predict the wrong site preference for the He interstitial defect and significantly overestimate the binding energy of one He atom with a vacancy (1He–vacancy cluster, which is He in a substitutional position). These properties may affect the transport and accumulation of He and vacancies in the form of pressurized gas bubbles in the Fe matrix and, consequently, the behavior of structural materials under irradiation. It therefore becomes obvious that new efforts should be made using the modern developments in electronic structure calculations and classical simulations. In this paper we describe results of electronic structure calculations for small He clusters. We considered two He atoms in the interstitial area and up to three He atoms placed into a vacancy. However, electronic structure calculations cannot practically be extended further at this time. The size of the computational supercell required to provide a reasonable atomic relaxation increases with the size of the defect which is, in the case considered here, the number of helium atoms. Therefore, electronic structure calculations become tremendously time-consuming for the case of several He atoms. On the other hand, the DFT results obtained for small He clusters can be extrapolated to the case of a large helium local density using a multi-scale approach. In this paper we present a simple computationally efficient Fe–He potential fitted to reproduce formation and relaxation energies obtained from the first principles results. This potential was used to study He–vacancy cluster stability at zero temperature using the classical molecular statics (MS) technique.

2. Methodology

In a continuation of our previous work [13], the electronic structure calculations have been performed using the Vienna ab initio simulation package VASP [17,18]. Solution of the Kohn–Sham equations [16] was carried out self-consistently using a plane-wave basis set with PAW pseudopotentials [19,20]. Exchange and correlation functionals were taken in a form proposed by Perdew and Wang (PW91) [21] within the generalized gradient approximation (GGA). We present the results for a 54- and 128-atom supercells. One of the important parameters in our calculations is the cutoff energy, which determines the size of the plane-wave basis set. The convergence of the total energy with respect to the energy cutoff was carefully tested. We have found that the cutoff energy of 350 eV is sufficient for a defect containing two He atoms. However, for more complicated defects such as a defect consisting of three He atoms in one vacancy, we had to increase the cutoff energy up to 380 eV to eliminate the noise in the forces caused by basis incompleteness. For the 54-atom supercell, we used from 32 to 52 k-points in the irreducible wedge depending on the defect configuration. For the 128-atom supercell, the number of k-points varied between 21 and 27. For all He defects we performed a full relaxation of the atomic positions and of the volume and shape of the supercell.

To avoid any confusion, we outline the definitions of the terms used in this paper. The relaxation energy of a crystal is determined as a difference between the total energy of a crystal before relaxation and that after. Similarly, the relaxation volume is a change of the supercell volume caused by the relaxation. The atomic configuration considered before relaxation corresponds to iron bcc crystal with an equilibrium lattice parameter of 2.827 Å and He atoms located at the same positions as we find them after relaxation. In this case the relaxation energy represents the decrease of the total energy of the crystal due to the relaxation of Fe atoms around He defects. The formation energy of the defect is given by

$$E^{\mathrm{f}}_{\mathrm{defect}} = E_{N\mathrm{Fe},M\mathrm{He}} - N \cdot E_{\mathrm{Fe}} - M \cdot E_{\mathrm{He}}, \qquad (1)$$

where N and M are the numbers of Fe and He atoms in the supercell, respectively, $E_{N\mathrm{Fe},M\mathrm{He}}$ is the total energy of the supercell with the defect, E_{Fe} is the total energy per Fe in a perfect bcc lattice, and E_{He} is the total energy of an isolated He atom.

The binding energy of N He interstitial atoms is defined as the energy required to move these atoms into infinitely separated interstitial positions. It is given by

$$E^{b}_{N\text{He-int}} = E_{N\text{He-int}} - NE_{\text{He-int}}, \quad (2)$$

where $E_{N\text{He-int}}$ and $E_{\text{He-int}}$ are the total energies of supercells with N and one He interstitial, respectively. The binding energy of an atom i to a He–vacancy cluster is determined by

$$E^{b}_{i} = E_{Ni,Mj} - E_{(N-1)i,Mj} - E_{i\text{-int}}, \quad (3)$$

where $E_{Ni,Mj}$ is the total energy of a crystal consisting of N atoms of type i and M atoms of a type j and $E_{i\text{-int}}$, is the total energy of the supercell with an i type of interstitial. The migration energy of an interstitial is determined as the energy barrier which the atom has to overcome in passing from one stable interstitial position to another.

3. Results

3.1. DFT calculations

We considered three different defect configurations: two He atoms placed in an interstitial position (2He), and either two or three He atoms located inside one vacancy (2He–vac and 3He–vac). Two He atoms were put inside the vacancy in the form of a dumbbell in three different orientations: along the ⟨1 0 0⟩, ⟨1 1 0⟩ and ⟨1 1 1⟩ principal crystal axes. For three He atoms, we considered only one configuration, an isosceles triangle lying in the {1 1 0} plane. For these configurations we calculated the relaxation and formation energy, volume dilatation and relaxed position of He atoms. The results of calculations for 54- and 128-atom supercells are presented in Table 1. We also include previously published [13] results for the He tetrahedral interstitial. First, one can see that all He defects produce strong lattice relaxation. The displacements of Fe atoms at the supercell boundary show that the supercells employed are not large enough to reach complete atomic relaxation. Increasing the supercell size from 54 to 128 atoms decreases the formation energies of the defects by 0.1–0.4 eV and also reduces the dilatation of the supercell volume. The largest decrease of the formation energy corresponds to two He interstitials. Nevertheless, if one compares the energy values energy obtained for the same computational settings, the relationship between the energies changes insignificantly. Thus, our results are reliable to make some important conclusions. For example, the binding energy of two He interstitials obtained using a 54-atom supercell is equal to 0.03 eV. For 128 atoms, the value is 0.02 eV. Both these numbers lie near the limit of the computational accuracy of the method and we conclude that He interstitials are bound to each other extremely weakly.

The formation energy of a 2He–vacancy complex depends insignificantly on the He atoms orientation indicating that this complex is likely to rotate inside the vacancy. For ⟨1 1 0⟩ and ⟨1 1 1⟩ dumbbell the formation energies differ by only 0.02 eV. The formation energy is slightly higher for the ⟨1 0 0⟩ dumbbell. The volume expansion of the supercell changes linearly with the number of He atoms inside the vacancy. The formation volume of an isolated vacancy is -0.25Ω, where $\Omega = 11.297$ Å^3 is the equilibrium atomic volume in bcc iron. When one He atom is placed into the vacancy, the supercell volume gets restored to its equilibrium value [13]. When the number of He atoms inside the vacancy

Table 1
DFT results for small He clusters and He tetrahedral interstitial

		2He	2He–vac [1 0 0]	2He–vac [1 1 0]	2He–vac [1 1 1]	3He–vac	He int[a]
54 atoms	R, Å	1.60	1.53	1.55	1.55	1.56, 1.61, 1.61	–
	ΔV, Ω	1.32	0.35	0.30	0.30	0.76	0.70
	E^{rel}, eV	3.55	0.73	0.75	0.69	1.03	1.07
	E^{f}, eV	9.15	7.12	6.95	6.97	9.68	4.59
128 atoms	R, Å	1.60	–	1.55	–	1.56, 1.61, 1.61	–
	ΔV, Ω	1.22	–	0.27	–	0.66	0.51
	E^{rel}, eV	4.06	–	0.74	–	1.20	1.29
	E^{f}, eV	8.72	–	6.63	–	9.44	4.37

R is a He–He separation, ΔV is a volume change during atomic relaxation, E^{rel} and E^{f} are relaxation and formation energies of the defects, Ω is iron equilibrium atomic volume equal to 11.297 Å^3.

[a] The results for He tetrahedral interstitial in 128-atom supercell were published in [13].

changes from two to three, the volume expansion increases from 0.27Ω to 0.66Ω. In all cases considered, the equilibrium spacing between He atoms, 1.5–1.6 Å, is significantly shorter then the spacing between He–He atoms in vacuum which is equal to 2.97 Å [22].

3.2. Interaction potentials for He in the Fe matrix

The results of first principles calculations were used as input for the development of empirical potentials for Fe–He and He–He interactions in the iron matrix described by a particular Fe potential from the literature. Our objective was to fit formation and relaxation energies of the following six configurations: He interstitial in octahedral and tetrahedral positions, single He substitutional defect and the three helium clusters (2He, 2He– and 3He–vacancy) described above. The full set of potentials necessary for classic atomistic simulation includes description of Fe–Fe, Fe–He and He–He interactions. For this purpose, we have initially used the well-known Finnis–Sinclair many-body potential that reasonably reproduces the basic properties of alpha-iron [23], although it overestimates the formation energies of Fe SIAs in comparison with DFT–GGA calculations [24]. Note that the Finnis–Sinclair potential has also been using in combination with Wilson's Fe–He potential in earlier studies of helium in iron [6,7]. Therefore, using the Finnis–Sinclair potential provides a comparison of our results with the results of previous simulations. It is important to note that the technique we use to obtain the Fe–He cross potential can be applied to any other iron matrix potential, and we are in the process of applying this approach with more recent iron potentials.

Since our aim is to obtain an Fe–He potential fitted to the properties of multiple He–atom clusters, we need to first define the He–He potential in bulk iron. To this end, we performed ab initio calculations for an unrelaxed bcc iron lattice with 128 Fe atoms in the supercell and with two He interstitials in their most stable position, i.e. in tetrahedral sites. It was assumed that the Fe–He interaction is short-range and therefore, due to symmetry, the forces acting on He atoms from Fe atoms are the same for the both He atoms and do not affect the force that one He atom experiences from the other. By placing two He interstitials at different distances from each other one can obtain the distance dependence of the He–He effective force. The He–He effective interaction energy can also be calculated if one subtracts twice the total energy of a single He tetrahedral defect from the total energy of a crystal with two He interstitials. The above technique allows the effective force and interaction energy to be obtained independently without making any assumptions about the He–He potential model. The obtained distance dependence of the He–He effective interaction energy and the effective force are presented in Fig. 1(a) and (b), respectively. For comparison we show the He–He interaction energy and force received from ab initio calculations in vacuum [25]. One can see that at short distance, <2 Å, the He–He effective interaction in iron is very similar to the He–He interaction in vacuum. Since the d-electrons of iron are well localized, the electronic charge density is low in the interstitial area and it has a small effect on the repulsion between

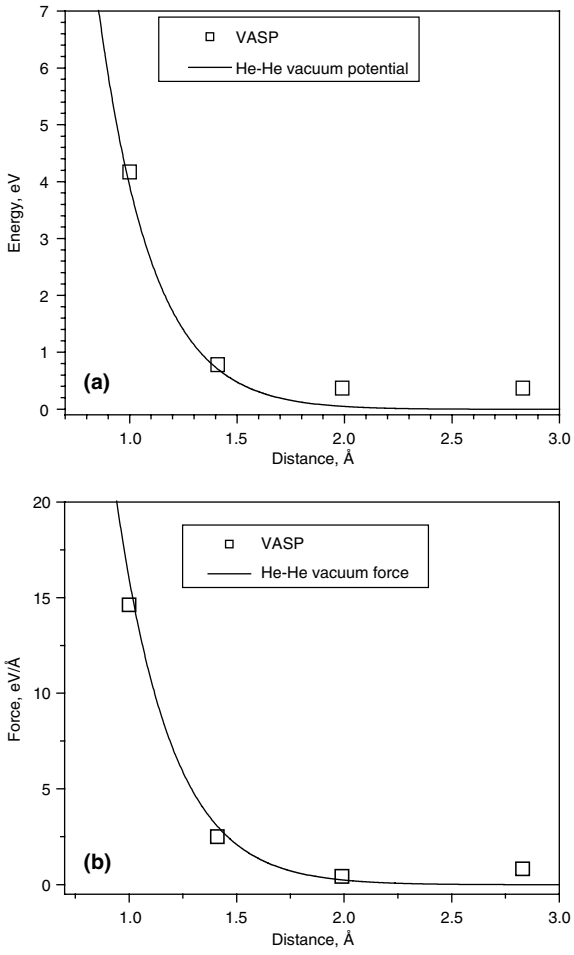

Fig. 1. (a) Effective interaction energy and (b) effective force dependence versus distance between He atoms.

He cores. However, the He–He interaction in vacuum becomes extremely weak at distances larger than 2 Å, while remaining noticeably stronger in the iron matrix. Interatomic separations larger then a lattice parameter were not considered in our ab initio calculations, since the results can be affected by He–He interaction through the boundaries of the simulated 128-atom supercell. In general, we conclude that He–He interaction in the iron crystal can be reasonably well represented by the pair potential [25] calculated for the vacuum.

The interaction between He and Fe atoms is more complex. As discussed previously [26], it is unlikely that a pair-potential function can describe both the formation and relaxation energies of He defects in iron simultaneously. The physical reason for this difficulty is a change of the magnetic moment of the neighboring Fe atoms produced by the He defect. In the language of potentials this is because the Fe–He interaction energy and force depend not only on the distance between Fe and He atoms but also on the environment of each of them. In other words, one must include a many-body interaction part in the Fe–He potential.

To simplify future applications of the empirical Fe–He potential we have chosen the same model as used for the matrix iron potential [23] which is the well-known many-body formalism introduced by Finnis and Sinclair. Then, the total energy of an Fe–He system is written as

$$E = \sum_i A_i \sqrt{\rho_i} + \sum_{i,j \neq i} V(r_{ij}), \tag{4}$$

where the first term represents an attractive many-body interaction which provides cohesion and the second term is a repulsive pair potential. The first sum is carried over the atoms in the supercell; the second sum is performed over the total number of the interacting atomic pairs. The A_i coefficient depends on the atom type and ρ_i is the surrounding atomic density that is given by the sum of the atomic density functions, $\Psi(r_{ij})$

$$\rho_i = \sum_{j \neq i} \Psi(r_{ij}). \tag{5}$$

For the density function, $\Psi(r_{ij})$, and pair-potential function, $V(r_{ij})$, we choose a simple and relatively flexible mathematical form which is

$$F(r_{ij}) = p_1 \left(1 - p_2 \left(\frac{r_{ij}}{p_3} - 1\right)\right) e^{-p_4 \left(\frac{r_{ij}}{p_3} - 1\right)} \cdot f_{\text{cut}}(r_{ij}), \tag{6}$$

where $f_{\text{cut}}(r_{ij})$ is a cutoff function whose first and second derivatives vanish when $r_{ij} = r_b$ and $r_{ij} = r_c$:

$$f_{\text{cut}}(r_{ij}) = (1-x)^3(1+3x+6x^2), \quad \text{where} \quad x = \frac{r_{ij} - r_b}{r_c - r_b}. \tag{7}$$

For $r_{ij} < r_b$, $x = 0$ and for $r_{ij} > r_c$, $x = 1$. Eq. (6) indicates that $F(r_{ij})$ has four fitting parameters; however, p_3 is simply a scaling factor leaving only three free parameters. Depending on their values, the function can be either continuously decreasing or increasing. It may also have one extremum. Overall, there are seven free fitting parameters describing the Fe–He interaction. They are found by fitting 12 energies obtained from the first principles calculations. First, we had to reduce the discrepancies between DFT calculations and Finnis–Sinclair potential for pure iron. The equilibrium lattice parameter for iron calculated by DFT is equal to 2.827 Å, while the Finnis–Sinclair potential gives a value 2.8665 Å. A similar discrepancy arises when we consider vacancy formation energy. The DFT calculated value is 2.07 eV and the Finnis–Sinclair potential gives 1.83 eV. Since we are interested in He defect calculations in a Finnis–Sinclair matrix, the values obtained for the structures considered in DFT calculations were rescaled. In the case of He defects located in iron vacancies, we subtracted 0.24 eV from the formation energies of the defects. Thus, in our fitting scheme the primary formation energies of two and three He atoms in a vacancy were equal to 6.59 eV and 9.20 eV, respectively.

The parameters were fitted using a least-squares method. Our fitting database included 12 formation energies corresponding to six selected He defect configurations with relaxed and unrelaxed structures calculated by VASP. Initial guesses for the potential parameters $\{A_{\text{He}}, f_i\}$ were used to estimate the sum of squared differences. The minimization of the sum of squared differences was performed by the conjugate-gradient method. However, this procedure does not guarantee zero forces for the relaxed configurations. Therefore, the obtained potential function was used to relax the above configurations by classical MS in the same 128-atom crystal with periodic boundary conditions. The parameters $\{A_{\text{He}}, f_i\}$ were then varied and relaxation repeated until the sum of squared differences between ab initio and MS simulations reaches its minimum. The calculated values of the parameters, $\{f_i\}$, are shown in Table 2. The parameter A_{He} in Eq. (4) was found to be equal to 0.087783 eV/Å. The density functions

Table 2
Parameters for density function and pair potential given by Eq. (6)

	f_1	f_2	f_3	f_4	r_b	r_c
Density function	15.855398 Å^2	−34.814838	0.537171 Å	2.359959	3.2 Å	3.9 Å
Pair potential	0.327625 eV	−0.089017	2.514731 Å	6.877193	3.2 Å	3.9 Å

The units of the parameters are specified for each case.

and pair potentials for the Fe–He system are presented in Figs. 2 and 3, respectively, together with Wilson's pair potential for comparison.

Although, our system of equations is over determined, we were able to fit first principles energies with reasonably high accuracy. The results of the fitting procedure for a single He defect and small He clusters are presented in Tables 3 and 4, respectively. Unless specified, the calculations were performed for 128-atom supercell. In Table 3 one can see that the fitted empirical potential reproduces the preference order for a single He defect. The relaxation energies are described with less accuracy than the formation energies of the unrelaxed structures. Note that the relaxation energy included in Table 3 for the tetrahedral He defect (1.29 eV) represents a correction from our previously published value [13]. In Fig. 4 we present the profile of the formation energy of a He interstitial defect along a [100] path in the unrelaxed iron lattice. One can see that the new empirical potential reproduces the energy profile extremely well, even though intermediate He positions along the path were not included in the fitting procedure. We also tested how well the new potential describes the effective force exerted by a He interstitial on the iron sites in unrelaxed lattice. The dependence of the effective force on the distance between an Fe atom and a He interstitial is presented in Fig. 5. The new potential reproduces the effective Fe–He force reasonably well except for

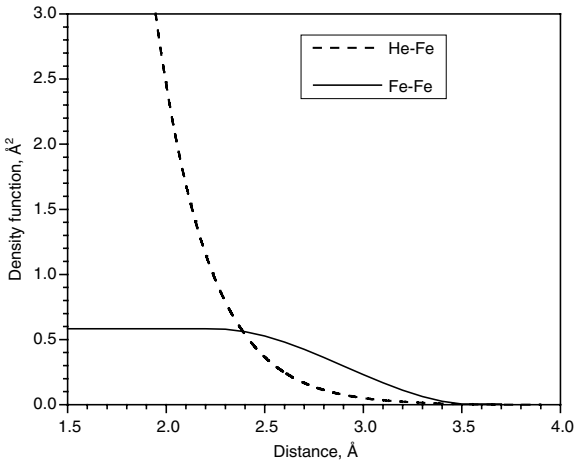

Fig. 2. The density functions, $\Psi(r)$ (Eq. (5)), for Fe–He interaction and Fe–Fe interaction in Finnis–Sinclair model [23].

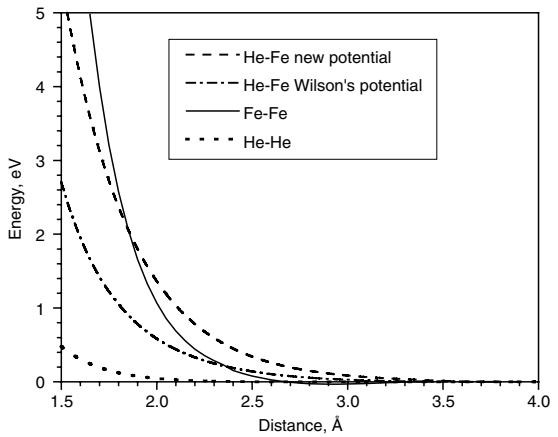

Fig. 3. The repulsive pair potentials, $V(r)$ (Eq. (4)), for Fe–He interaction, Fe–Fe Finnis-interaction in Finnis–Sinclair model [23] and He–He interaction [24].

Table 3
Relaxation and formation energies measured in eV of single He defect in iron calculated from the first principles and using fitted empirical potential

	He_{octa}		He_{tetra}		He_{sub}	
	E^{rel}	E^f	E^{rel}	E^f	E^{rel}	E^f
VASP [13]	1.76	4.60	1.29	4.37	0.32	3.84
Fe–He potential	1.83	4.54	1.15	4.50	0.15	3.91

E^f of He_{sub} was shifted according to the text.

Table 4
He–He separation, relaxation and formation energies of He clusters in iron calculated using fitted empirical potential

	2He	2He–vac	3He–vac
R, Å	8.79	1.53	1.63, 1.63, 1.63
E^{rel}, eV	1.68	0.43	1.55
E^f, eV	8.79	6.61	9.28

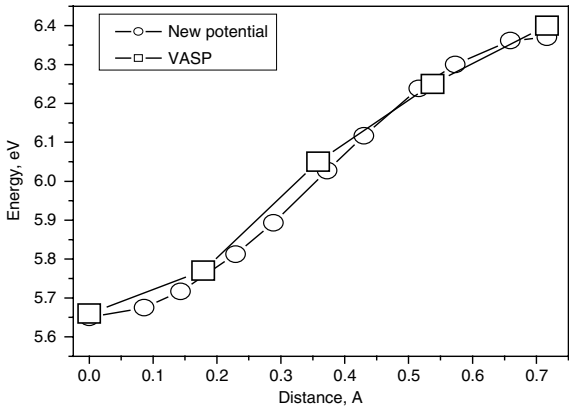

Fig. 4. He interstitial defect energy profile along [1 0 0] direction from He tetrahedral to He octahedral defect in the iron unrelaxed lattice. VASP calculations were performed for 54-atom supercell.

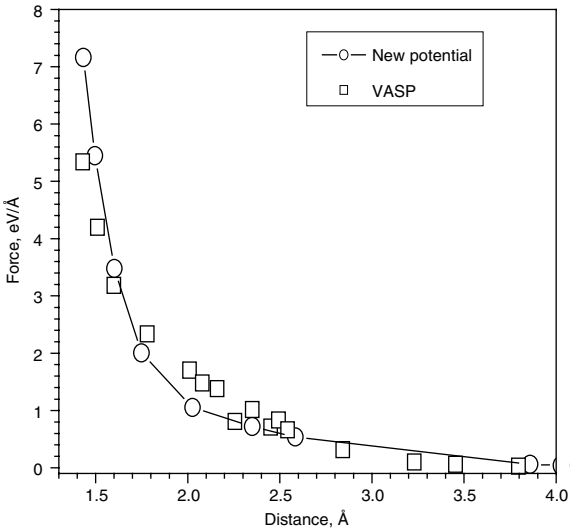

Fig. 5. The effective force exerted on neighboring Fe atoms by He interstitial defect in unrelaxed lattice.

very short separation distances, which causes the above-mentioned disagreement in relaxation energies. The formation energies of the relaxed structures are fitted to within an accuracy of 0.13 eV. The maximum energy deviation is obtained for the He tetrahedral defect.

The accuracy of the fitted properties for the He clusters shown in Table 4 is satisfactory. The formation energy of two He interstitials obtained with the new potential differs by 0.07 eV from the results presented in Table 1. Taking into account that the formation energy of the He interstitial is also reproduced with some inaccuracy, the binding energy of two He interstitials, which is equal to 0.21 eV, appears to be somewhat overestimated. The accuracy of the new potential is least accurate at describing the properties of He in the interstitial region. However, since helium is easily trapped by vacancies and exhibits rapid interstitial migration, the deficiency of our potential in describing He properties in the interstitial region should have only a weak effect on its application to future simulations involving He–vacancy-type defects. The formation energies of He atoms placed in a vacancy are slightly overestimated compared with the shifted results of ab initio calculations. For two and three He atoms inside a vacancy, the formation energy received with the new potential differs from their ab initio values by 0.22 eV and 0.08 eV, respectively. The values of the formation energies presented in Tables 3 and 4 are found to be slightly lower when the simulations have been performed on larger supercells.

3.3. Static properties of multiple He–vacancy clusters

The newly obtained Fe–He potential was used to study He–vacancy cluster stability at 0 K. We considered an iron bcc crystal with one vacancy and up to 10 He atoms placed inside it. Periodic boundary conditions were applied to a $10a_0 \times 10a_0 \times 10a_0$ computational cubic box ($a_0 = 2.8665$ Å is bcc iron equilibrium lattice parameter). The atomic coordinates were relaxed using a conjugate-gradient method to zero force at constant volume. We observed a strong atomic relaxation around the He–vacancy complex. When the number of He atoms in a vacancy is equal to seven, the local forces produced by the He–vacancy complex are strong enough to cause the formation of an Fe SIA. The displacement of the first neighbor Fe from its lattice site reaches 0.41 Å, which is 14% of the lattice parameter. We studied the dependence of the binding energy of a He atom to a He–vacancy cluster versus the cluster size using Eq. (3). In the extreme case, when the number of He atoms inside the vacancy is equal to zero, we considered the binding energy of He atom to the vacancy. We also studied the case when a He–vacancy cluster forces the emission of the neighboring Fe atom into an interstitial position, and calculated the binding energy of the Fe SIA to the remaining He–di-vacancy cluster. The results for the He atom and Fe SIA are presented in Fig. 6(a) and (b), respectively. The abscissa in Fig. 6(a) denotes the number of He atoms in the

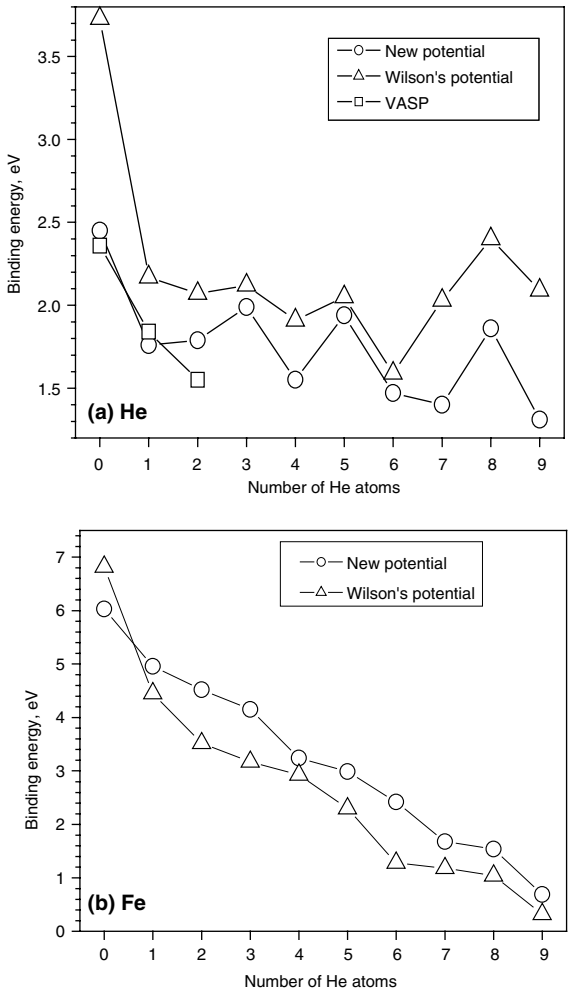

Fig. 6. Binding energy of (a) a He atom to the He–vacancy cluster and (b) an Fe SIA to the He–di-vacancy cluster versus the number of He atoms inside the vacancy.

cluster before the next He is bound. Thus, the value for the first He bound to the vacancy is shown at zero. The corresponding energies obtained from Wilson's Fe–He pair potential are also presented for comparison. In Fig. 6(a) we also show the binding energies for the 2He– and 3He–vacancy complexes calculated from first principles. One can see that the results obtained with the new potential for the binding of small He clusters inside a vacancy are in very good agreement with ab initio calculations. Only for the case of the 3He–vacancy cluster is the binding energy overestimated by as much as 0.25 eV.

Comparison with Wilson's potential in Fig. 6(a) demonstrates that it systematically overestimates the binding of a single He atom to the vacancy. The discrepancy is 1.3 eV and is a significant deficiency of Wilson's potential. Another feature of the new Fe–He potential is that it gives strong preference for symmetric configurations. Wilson's pair potential can only poorly reproduce this preference for the symmetric configurations due to its spherically symmetric, purely repulsive nature. The binding energy of a He atom to the cluster changes from 1.75 eV to 2.0 eV, when the size of cluster goes from 3 to 4 atoms. This corresponds to formation of a tetrahedral He structure inside the vacancy. Another peak at 6 He atoms is related to formation of an octahedron. When the seventh He atom is added to the He–vacancy cluster, it is ejected to an interstitial position 1.5 Å away from the vacancy center. All subsequent atoms are also pushed into the interstitial region nearby the vacancy center. The binding energy of a He atom to the He–vacancy cluster changes irregularly depending on the number of He atoms. However, it remains high, indicating that He-clusters should remain stable up to high temperatures which is also in agreement with experimental observations [2,3]. At the same time, the binding energy of an Fe SIA to the cluster decreases continuously as the number of He atoms increases and for the 9He–di-vacancy complex it reaches 0.7 eV. Wilson's potential predicts the same dependence of the binding energy of the Fe SIA on the cluster size, but systematically underestimates the absolute value of the energy.

As seen in Fig. 6(a), the lowest binding energy occurs for the case of a 9He–vacancy cluster and is equal to 1.31 eV. Using this value one can estimate the activation energy for helium desorption, defined as a sum of binding and He interstitial migration energies. The migration energy of the He interstitial was calculated by moving a He defect from a tetrahedral to an octahedral site along a [1 0 0] path and performing complete atomic relaxation at each position. It was found to be the same as the difference between the formation energies of He octahedral and tetrahedral interstitials, namely 0.04 eV. Thus, the calculated desorption activation energy is equal to 1.35 eV. The value found from the desorption experiments is 1.4 ± 0.3 eV [3]. While the calculated and experimentally measured values are very similar, more simulations have to be done to confirm this agreement. The simulations must be performed at experimental conditions that include high temperature and with the correct He–vacancy ratio. Since the mass of a He atom is about ten times smaller than the mass of an Fe atom, the

results of molecular dynamics simulation can be very different from the one obtained in our static picture. Looking only at the binding energies at zero temperature, we can make a few conclusions. One of the important results of our simulations is the reduction in Fe SIAs binding energy with the number of He atoms. This is a necessary condition for He-bubbles to grow inside the iron matrix. Earlier calculations also suggested that highly pressurized bubbles could emit interstitials and/or punch small interstitial loops [27,28]. Using the data from Fig. 6(b) one can expect that in the case of 10 He atoms inside a vacancy an Fe SIA can be emitted. Internal thermal pressure due to the He–He interaction should shift all the critical processes towards a lower He-to-vacancy ratio.

4. Conclusions

A multi-scale approach has been applied to study He cluster properties in iron. Electronic structure calculations were performed for up to three He atoms inside a single vacancy. These results were used to fit a new empirical many-body Finnis–Sinclair type potential for He in an iron matrix. The potential reproduces formation and relaxation energies of single He and small He clusters with a good accuracy. We used the potential to study zero temperature stability of helium clusters in a vacancy. The binding of an Fe self-interstitial to the helium–di-vacancy cluster decreases linearly with the increase of the cluster size, while He atoms remain bound to the He–vacancy cluster with an energy higher then 1.3 eV. The He-cluster binding energy also depends strongly on the number of He atoms in the cluster. The fact that the binding energy of a He atom to the He–vacancy cluster never goes to zero reflects the weak He–He interactions in comparison with Fe–He. This is a necessary condition for substantial accumulation of He inside vacancy clusters. This stability provides a driving force for helium bubbles growth and swelling under irradiation when He is produced in the matrix.

The newly developed Fe–He potential is simple and efficient for application in molecular dynamics simulations. However, it was developed for an iron matrix described by Finnis–Sinclair potential that overestimates the formation energies of Fe SIAs and the activation energy of vacancy migration. This sets some limitations on the problems that can be considered using the new potential. In further work, the fitting scheme presented in this paper will be used to obtain another Fe–He potential based on the iron potential recently developed by Mendelev et al. [29].

Acknowledgements

This research was sponsored by the Division of Materials Sciences and Engineering (Seletskaia, Osetsky, and Stocks) and the Office of Fusion Energy Sciences (Stoller), US Department of Energy, under contract DE-AC05-00OR22725 with UT-Battelle, LLC.

References

[1] R.E. Stoller, J. Nucl. Mater. 174 (1990) 289.
[2] M.B. Lewis, K. Farrell, Nucl. Instrum. and Meth. B 16 (1986) 163.
[3] R. Vassen, H. Trinkaus, P. Jung, Phys. Rev. B 44 (1991) 4206.
[4] R.E. Stoller, G.R. Odette, J. Nucl. Mater. 131 (1985) 118.
[5] F.A. Garner, D.S. Gelles, in: N.H. Packan, R.E. Stoller, A.S. Kumar (Eds.), Effects of Radiation on Materials, ASTM, Philadelphia, 1990, p. 673.
[6] W.F.W.M. Van Heugten, F.V.D. Berg, L.M. Caspers, A. Van Veen, Delft Progr. Rep. 3 (1978) 97.
[7] L.M. Caspers, M.R. Ypma, A. Van Veen, G.J. Van der Kolk, Phys. Status Solidi (a) 63 (1981) K183.
[8] K. Morishita, R. Sugano, B.D. Writh, T. Diaz de la Rubia, Nucl. Instrum. and Meth. B 202 (2003) 76.
[9] M. Manninen, J.K. Norskov, C. Umrigar, J. Phys. F: Met. Phys. 12 (1982) L7.
[10] B. Bech Nielsen, A. van Veen, J. Phys. F: Met. Phys. 15 (1985) 2409.
[11] W.D. Wilson, in: F.W. Young, M.T. Robinson, (Eds.), Conference on Fundamental Aspects of Radiation Damage in Metals, USERDA-CONF-751006-P2, vol. 1025, 1975.
[12] P.T. Wedepohl, Proc. Phys. Soc. 92 (1967) 79.
[13] T. Seletskaia, Y. Osetsky, R.E. Stoller, G.M. Stocks, Phys. Rev. Lett. 94 (2005) 046403.
[14] C.C. Fu, F. Willaime, J. Nucl. Mater., these proceedings.
[15] P. Hohenberg, W. Kohn, Phys. Rev. B 136 (1964) 864.
[16] W. Kohn, L.J. Sham, Phys. Rev. 140 (1965) A1133.
[17] G. Kresse, J. Hafner, Phys. Rev. B 47 (1993) 558; G. Kresse, J. Hafner, Phys. Rev. B 49 (1994) 14251.
[18] G. Kresse, J. Furthmüller, Phys. Rev. B 54 (1996) 111698.
[19] P.E. Blöchl, Phys. Rev. B 50 (1994) 17953.
[20] G. Kresse, J. Joubert, Phys. Rev. B 59 (1999) 1758.
[21] J.P. Perdew et al., Phys. Rev. B 46 (1992) 6671; J.P. Perdew et al., Phys. Rev. B 48 (1993) 4979(E).
[22] J.F. Olgivie, F.Y.H. Wang, J. Mol. Struct. 273 (1992) 277; J.F. Olgivie, F.Y.H. Wang, J. Mol. Struct. 291 (1993) 313.
[23] M.W. Finnis, J.E. Sinclair, Philos. Mag. A 50 (1984) 45.
[24] C.-C. Fu, F. Willaime, P. Ordejon, Phys. Rev. Lett. 92 (2004) 175503.
[25] R.A. Aziz, A.R. Janzen, M.R. Moldover, Phys. Rev. Lett. 74 (1995) 1586.

[26] T. Seletskaia, Yu.N. Osetsky, R.E. Stoller, G.M. Stocks, in: Second International Conference on Multiscale Materials Modeling, October 11–15, 2004, Los Angeles, CA.
[27] B.B. Glascow, W.G. Wolfer, J. Nucl. Mater. 122&123 (1984) 503.
[28] H. Trinkaus, W.G. Wolfer, J. Nucl. Mater. 122&123 (1984) 552.
[29] M.I. Mendelev, S. Han, D.J. Srolovitz, G.J. Ackland, D.Y. Sun, M. Asta, Philos. Mag. 83 (2003) 3977.